Resistance of the Bianthrone Radical Anion toward Oxidation by Dioxygen

Saba M. Mattar,* Ramaswami Sammynaiken, and Alyson D. Stephens

Centre for Laser Applications and Molecular Science and Department of Chemistry, University of New Brunswick, Fredericton, New Brunswick, Canada E3B 6E2

Received: June 17, 1997; In Final Form: August 5, 1997[⊗]

The full geometry optimization of the **A** and **B** forms of bianthrone and their eight corresponding ions has been performed. From the resulting molecular structure parameters, some structure-bonding relationships are established. The calculated electron affinities, which take into account internal reorganizational energies, suggest that the bianthrasemiquinone radical anion $\mathbf{B}^{\bullet-}$ may be the first semiquinone that is stable toward oxidation by dioxygen. This is experimentally proven using electron paramagnetic resonance (EPR) spectroscopy. The $\mathbf{B}^{\bullet-}$ radical anion, prepared via the addition of NaOH to **B** in dimethyl sulfoxide (DMSO) solution, displays a strong well-resolved EPR spectrum. From the simulation of the spectrum and analysis of the line widths, the bimolecular rate constant for the spin−spin exchange between two $\mathbf{B}^{\bullet-}$ radicals is determined to be 3.19×10^9 L mol^{-1} s^{-1}. When the solvent is saturated with O_2, evidence for the close proximity and the frequent encounters between the radical and O_2 is apparent from the large broadening of the hydrogen hyperfine splittings. The magnitude of the line width broadening reveals that the Heisenberg spin−spin exchange between $\mathbf{B}^{\bullet-}$ and O_2 is approximately 10% less efficient than that of neutral nitroxide spin labels. This suggests that the DMSO solvation sphere surrounding the $\mathbf{B}^{\bullet-}$ radical anion protects it and slightly decreases its collision frequency with O_2. When the O_2 is expelled from solution, the EPR spectrum reverts to its normal well resolved form with no measurable loss of intensity. The unusual stability of $\mathbf{B}^{\bullet-}$ is attributed to the delocalization of its unpaired type electron over a major portion of this large anion.

Introduction

In this article we make use of electron paramagnetic resonance (EPR) spectroscopy to demonstrate that, although the bianthrasemiquinone radical anion $\mathbf{B}^{\bullet-}$ is in intimate contact with O_2 in solution, it is totally resistant to chemical oxidation. To the best of our knowledge, this is the first reported semiquinone radical anion that is stable in the presence of molecular dioxygen.

Organic molecules that undergo large internal rearrangements as a result of single electron transfer are rare and therefore of prime interest.[1] An excellent example of such a molecule is bianthrone.[1−3] It is a sterically hindered olefin that undergoes dramatic structural changes when heated, photolyzed, oxidized, or reduced. At ambient temperatures it is yellow and has the **A** conformation shown in Figure 1a. The anthrone components adopt a butterfly structure and are folded away from one another. This relieves the steric crowding between the 1,8′ and 8,1′ hydrogen atoms without significant twisting of the ethylenic bond formed between the 9 and 9′ carbon atoms. When heated, **A** transforms to the green **B** form which has planar anthrone units with more stable delocalized π-type orbitals (Figure 1b). This results in a twisted $C_9-C_{9'}$ double bond.[1−4]

In general, the total wave function of compounds with twisted ethylenic double bonds is expressed as a linear combination of Slater determinants[5]

$$\Psi = C_1|\ldots \psi_1 \overline{\psi_1}| + C_2|\ldots \psi_1 \overline{\psi_2}| + C_3|\ldots \overline{\psi_1}\, \psi_2| + C_4|\ldots \psi_2 \overline{\psi_2}| \quad (1)$$

where ψ_1 is the highest occupied one-electron molecular orbital (HOMO) and ψ_2 is the lowest unoccupied one-electron molecular orbital (LUMO). If the HOMO−LUMO gap is large, then

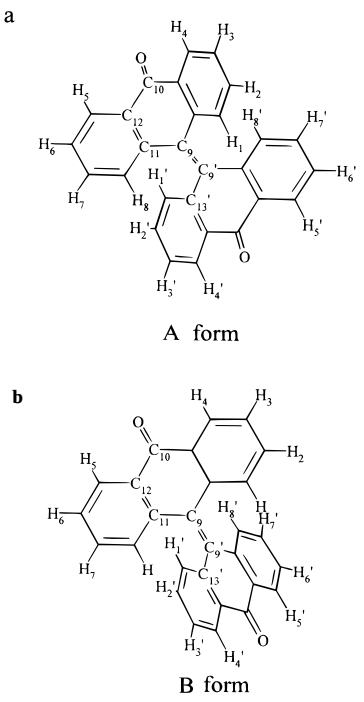

Figure 1. The **A** and **B** structures of bianthrone.

$C_1 \approx 1.0$ and $C_2 = C_3 = C_4 \approx 0.0$, giving a closed-shell singlet state. When the HOMO−LUMO gap is small two situations may arise. The first is when C_1 is comparable to $-C_4$ and $C_2 = C_3 \approx 0.0$. This leads to an open-shell singlet state. The second is when $C_1 = C_4 \approx 0.0$ and $C_2 \approx C_3$, leading to a triplet state. Therefore, it is of fundamental importance to determine the effects of using a multielectron configuration interaction wave function (eq 1) in the computation of the optimal geometry of **B** and its corresponding final ground state. If at its equilibrium geometry **B** has an open-shell singlet (biradical)

* To whom correspondence should be addressed.

[⊗] Abstract published in *Advance ACS Abstracts,* October 1, 1997.

S1089-5639(97)01966-X CCC: $14.00

ground state then it may have a detectable EPR spectrum. This spectrum should be different from that of the corresponding radical anion $\mathbf{B}^{\bullet-}$ or the 9,10-anthrasemiquinone radical, $\mathbf{AQ}^{\bullet-}$.

In both the **A** and **B** structures, the $C_9-C_{9'}$ bond plays an important and central role. Therefore, the properties of the resulting radical anions upon reduction of this bond have been extensively studied.[2−4,6−8] The simplest way to study the redox properties of bianthrone is by electrochemistry. On the basis of thermodynamic arguments, it is much easier to reduce the neutral **A** to the $\mathbf{B}^{\bullet-}$ radical anion directly.[1,3] It was experimentally found, however, that the large internal reorganizational energy (IRE) barrier in going from **A** to $\mathbf{B}^{\bullet-}$ causes the following two-step electron transfer mechanism, to be kinetically favored[1,3]

$$\mathbf{A} + e^- \rightarrow \mathbf{A}^{\bullet-} \quad (2)$$

$$\mathbf{A}^{\bullet-} \rightarrow \mathbf{B}^{\bullet-} \quad (3)$$

In addition, Olsen and Evans[3] have observed that as soon as the $\mathbf{A}^{\bullet-}$ is formed it is quickly reduced to $\mathbf{B}^{2-}$ because the reduction potential in reaction 2 is larger than that of

$$\mathbf{B}^{\bullet-} + e^- \rightarrow \mathbf{B}^{2-} \quad (4)$$

Direct simple electron transfer via an electrode is not the only means by which bianthrone may be reduced. Evans and Xie have predicted and demonstrated that **A** may be reduced to $\mathbf{B}^{2-}$ by means of quinone catalysts that have standard reduction potentials in the range of −0.5 to −1.0 V.[6,7]

Mattar and Sutherland have also demonstrated that **A** may be reduced to $\mathbf{B}^{\bullet-}$ and $\mathbf{B}^{\bullet-}$ to $\mathbf{B}^{2-}$ in distinct consecutive steps using NaOH in dimethyl sulfoxide (DMSO).[8] By monitoring the electronic absorption (UV−Vis) and EPR spectra as a function of the amount of NaOH in solution they concluded that both the **A** and **B** species are totally depleted before the $\mathbf{B}^{2-}$ dianion is formed. They also suggested that the reduction mechanism is probably that proposed by Sawyer and Roberts[9] where the OH^- was found to reduce a variety of benzoquinones, naphthaquinones and phenanthrones.[10,11] It is a two-step mechanism that starts with a reversible nucleophilic polar group coupling reaction between the OH^- and the neutral quinone in an aprotic solvent. The intermediate quinone−hydroxy complex then transfers an electron to another quinone forming the desired semiquinone radical anion.[9]

One of the side products of the Sawyer−Roberts reduction mechanism is H_2O_2, which in basic solutions decomposes to form O_2.[9] The O_2 could then cleave the $\mathbf{B}^{\bullet-}$ radical to yield $\mathbf{AQ}^{\bullet-}$ and eventually anthraquinone (**AQ**). Alternatively, it may leave the $C_9-C_{9'}$ bond intact and simply oxidize $\mathbf{B}^{\bullet-}$ to **B**, which in turn would convert to **A**. Consequently, as the next logical step, it is important to study the stability of the $\mathbf{B}^{\bullet-}$ radical toward O_2 in DMSO solutions when reduced by OH^-.

This paper is organized as follows. In the next section a brief explanation of the experimental apparatus and the computational details are given. The results of the full geometry optimization of the **A**, $\mathbf{A}^{\bullet-}$, $\mathbf{A}^{2-}$, $\mathbf{A}^{\bullet+}$, $\mathbf{A}^{2+}$, **B**, $\mathbf{B}^{\bullet-}$, $\mathbf{B}^{2-}$, $\mathbf{B}^{\bullet+}$, and $\mathbf{B}^{2+}$ species are then presented, and the structure-bonding relations of **B** and $\mathbf{B}^{\bullet-}$ are discussed. This is followed by the simulation and analysis of the experimental $\mathbf{B}^{\bullet-}$ EPR spectra in the absence and presence of O_2. From the line width analysis, it is shown that $\mathbf{B}^{\bullet-}$ undergoes frequent Heisenberg spin−spin exchange broadening due to the translational diffusion of the O_2 molecules in DMSO. This is followed by a summary of the conclusions derived from the total work.

Experimental and Computational Details

The custom-built EPR spectrometer and sample preparation have been previously described in detail.[8] Bianthrone, mesitylene, and DMSO were purchased from Aldrich Chemical Co. of Milwaukee, WI. The DMSO (HPLC grade, glass distilled, water content < 0.08%) was used without further purification. The bianthrone was recrystallized from mesitylene in the absence of light.

Solutions of oxygen-free and O_2-saturated 1.0 mM $\mathbf{B}^{\bullet-}$ were prepared by purging them with dry N_2 and O_2 gas, respectively, in the preparation vessel. To ensure that the purging process was complete, bubbling of the gas was maintained for at least 1 h. The solutions were then transferred to a flat flow-through quartz cell in the EPR cavity by means of Teflon tubing and a positive gas pressure. When changing the samples, care was taken to completely flush the cell with the new solution and to exclude any gas bubbles from the flat compartment.

Simulations, using pure Lorentzian line shapes, were carried out on a personal computer with a program written by one of the authors (SMM). The experimental and simulated spectra were scaled such that the total scan and peak-to-peak signal amplitudes were equal. The "goodness" of the fit was determined visually from the superimposed spectra.

The electronic structure computations were performed using the HyperChem and MOPAC7 suite of programs on an IBM RS/6000 model 355 workstation.[12] The semiempirical PM3 method[13] with limited CI was used to optimize the geometries. The geometry optimization process was terminated when the sum of the energy gradients was less than 0.001 kcal $Å^{-1}/mol^{-1}$. The uncertainties in the total energies were of the order of 1.0 kcal/mol while those of the bond distances were approximately 0.01 Å. Bond angles are accurate to within ±2.5°.

To ensure that the optimized geometries were not due to any transition states or saddle points on the potential energy surface, the first and second derivatives of the energy with respect to the normal mode displacements were also computed. From these, the vibrational frequencies were calculated and no imaginary frequencies, characteristic of transition states, were found.

Results and Discussion

When properties of molecules that possess large internal reorganizational energies such as bianthrone are computed, it is imperative that fully geometry-optimized structures be used. For example, if a neutral molecule undergoes a large structural change when ionized its first ionization potential is the total energy difference between each of the fully optimized structures (neutral molecule and cation).

Ab initio geometry optimizations that take into consideration the effects of configuration interaction for large molecules are still beyond present computer capabilities. As an alternative, semiempirical computations have been attempted previously for bianthrone and its ions, but due to their large sizes, only a partial geometry optimization was possible using the MNDO/3 method.[14] In the present study, the full geometry optimization of **A**, $\mathbf{A}^{\bullet-}$, $\mathbf{A}^{2-}$, $\mathbf{A}^{\bullet+}$, $\mathbf{A}^{2+}$, **B**, $\mathbf{B}^{\bullet-}$, $\mathbf{B}^{2-}$, $\mathbf{B}^{\bullet+}$, and $\mathbf{B}^{2+}$ is undertaken and the results are given in Table 1. The PM3 method used is an improved and reparametrized form of the AM1 technique of Dewar. It yields results that are closer to experiment than the CNDO, INDO and MINDO/3 techniques.[15] The table lists some selected structural parameters and total energies.

Table 1 shows that **A** has the shortest $C_9-C_{9'}$ bond distance and a corresponding bond order of 1.79. For a double bond that is unstrained and localized on two carbon atoms the bond order should be exactly 2.0. In this case, the bond order drops to 1.79 because the orbital is not localized on the C_9-C_9 bond alone. When **A** is reduced to the $\mathbf{A}^{\bullet-}$, $\mathbf{A}^{2-}$, $\mathbf{B}^{\bullet-}$, and $\mathbf{B}^{2-}$ anions, one or more electrons will occupy the LUMO which has

TABLE 1: Selected Structural Properties for Bianthrone and Its Ions[a]

	R (9−9′)	BO (9−9′)	R (9−11)	R (CO)	BO (CO)	θ^b	θ^c	θ_t^d	E_{tot} (eV)
A^{2-}	1.462	1.07	1.427	1.243	1.67	23.3	34.5	5.7	−4149.33
$A^{\bullet-}$	1.397	1.40	1.452	1.225	1.80	29.3	40.5	2.5	−4150.39
A	1.353	1.79	1.474	1.215	1.90	35.5	48.6	1.5	−4148.45
$A^{\bullet+}$	1.407	1.37	1.454	1.211	1.95	34.5	42.0	1.0	−4140.04
A^{2+}	1.483	1.05	1.430	1.209	1.97	34.1	38.3	3.0	−4128.38
B^{2-}	1.478	0.99	1.409	1.248	1.64	0.0	0.0	90.0	−4150.69
$B^{\bullet-}$	1.445	1.17	1.430	1.232	1.77	1.5	3.9	63.7	−4150.71
B	1.396	1.60	1.464	1.221	1.86	3.0	4.6	53.0	−4147.70
BCI	1.426	1.26	1.452	1.222	1.86	3.6	3.9	58.5	−4147.65
$B^{\bullet+}$	1.452	1.17	1.433	1.218	1.92	1.9	4.0	65.7	−4140.25
B^{2+}	1.493	0.98	1.413	1.213	1.95	0.0	0.0	90.0	−4129.64

[a] A complete list of the atomic *x*, *y*, and *z* coordinates are available upon request. All angles are in degrees and bond distances in angstroms. [b] Torsion angle formed between the C_5, C_{12}, C_{10} and O atoms. [c] Torsion angle formed between the C_8, C_{11}, C_9 and $C_{9'}$ atoms. [d] Twist angle between the two anthrone units.

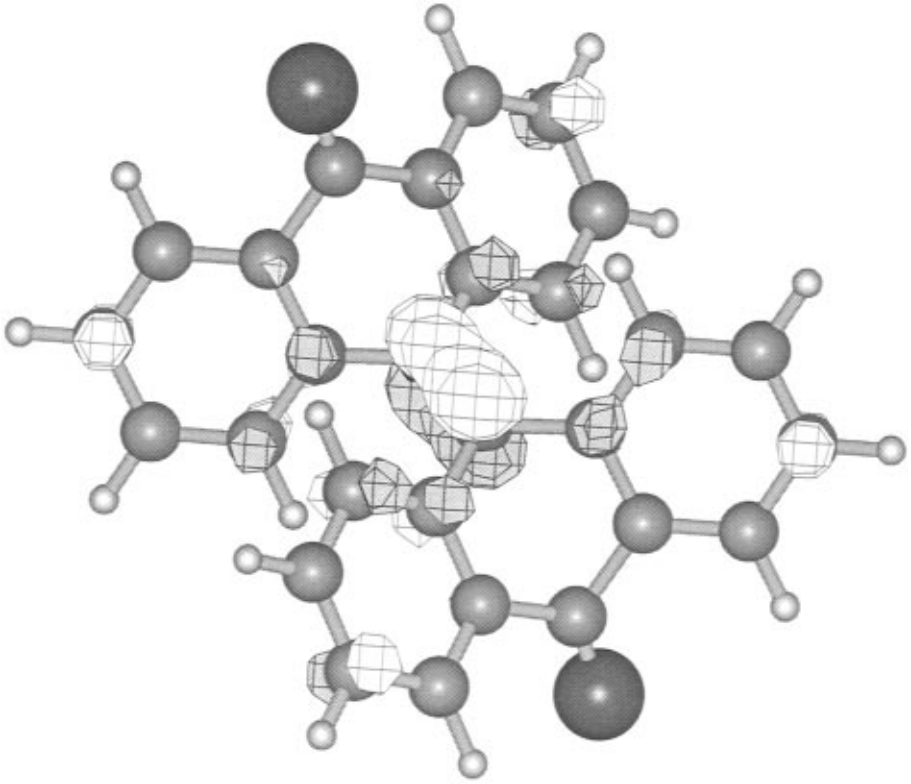

Figure 2. The three-dimensional plot of the **A** HOMO. The molecule has the same orientation as that of Figure 1a. The light colored isosurfaces represent the positive lobes while the darker ones are due to the negative lobes.

antibonding π^* character. This should lengthen the $C_9-C_{9'}$ bond distance and reduce the bond order. Indeed, Table 1 shows that the $C_9-C_{9'}$ bond orders of the $\mathbf{A}^{\bullet-}$ and $\mathbf{B}^{\bullet-}$ anions are 1.40 and 1.17, respectively. In the case of the $\mathbf{A}^{2-}$ and $\mathbf{B}^{2-}$ dianions, where two electrons are added to the LUMO, the $C_9-C_{9'}$ bond orders drop even further to 1.07 and 0.99, respectively, indicating that the bond is essentially a single bond.

Figure 2 shows the three-dimensional plot of the **A** HOMO. It is mainly C_9 and C_9 in character due to a bonding combination of the $2p_z(C_9)$ and $2p_z(C_{9'})$ orbitals. When the $\mathbf{A}^{\bullet+}$, $\mathbf{A}^{2+}$, $\mathbf{B}^{\bullet+}$, and $\mathbf{B}^{2+}$ cations are formed, one or two electrons are lost from the HOMO. This decreases the $2p_z(C_9)$ and $2p_z(C_{9'})$ contributions to the bonding also resulting in longer bond lengths and lower $C_9-C_{9'}$ bond orders (Table 1). In contrast, the HOMO has no carbonyl character. As is shown in Table 1, there is a negligible change in the C═O bond lengths and bond orders (1.90−1.97) when going from **A** to the cations.

Figure 3 displays the total energy of **B** as a function of the twist angle (θ_t) between the two anthrone halves. This angle is defined as the dihedral angle between the $C_{11}-C_9-C_{9'}-C_{13'}$ atoms. In curve a, all bond distances and angles were optimized except the dihedral angles that force the two anthrone halves to be planar. The minimum energy occurs around $\theta_t = 60$. The molecule is unrealistically destabilized at small twist angles because of the planarity of the anthrone units. When the dihedral angles are also optimized, curve b is obtained. It is substantially lower in energy, particularly for small twist angles, with an optimal θ_t of 53. To determine if post Hartree−Fock multiconfiguration interaction is needed to properly describe **B**, the geometry was fully optimized using the general CI wave function

$$\Psi = C_1|...\ 18b_3\ \overline{18b_3}| + C_2|...\ 18b_3\ \overline{18b_2}| + C_3|...\ \overline{18b}_3\ 18b_2| + C_4|...\ 18b_2\ \overline{18b_2}| \quad (5)$$

where the HOMO is the $18b_3$ MO and the LUMO is the $18b_2$ MO. Since the molecule has D_2 spatial symmetry, then by space

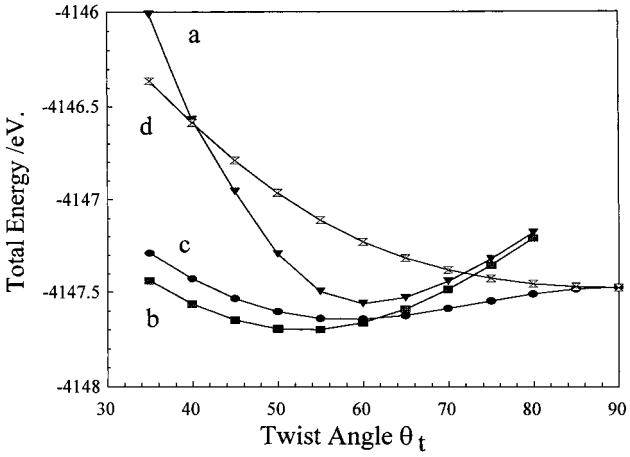

Figure 3. Total energy of **B** as a function of the twist angle, θ_t. (curve a) the dihedral angles that cause the two anthrone halves to be planar and θ_t are kept fixed while all other parameters are optimized. (curve b) All geometrical parameters except θ_t are optimized. (curve c) Same as curve b but optimizing the two configuration open-shell singlet state that transforms according to the A irreducible representation. (curve d) Same as curve b but optimizing the triplet state of B_1 symmetry.

and spin adaptation of the wave function one obtains the

$$X^1\Psi(A) = C_1|...\ 18b_3\ \overline{18b_3}| + C_4|...\ 18b_2\ \overline{18b_2}| \quad (6)$$

ground singlet state and the

$$a^3\Psi(B_1) = C_2|...\ 18b_3\ \overline{18b_2}| + C_3|...\ \overline{18b}_3\ 18b_2| \quad (7)$$

triplet state. These may be individually optimized and their total energies are given in curves c and d, respectively. They show that the open-shell singlet state is more stable than the corresponding triplet state over the entire range of θ_t. Although the optimal θ_t for curve c is 58.5°, the triplet has its most stable structure when $\theta_t = 90°$. At this angle both states are nearly degenerate and the singlet−triplet separation is negligible. Inspection of curves b and c shows that the minima only differ by approximately 0.07 eV (1.5 kcal/mol) while the optimal twist angles differ by 5.5°. Consequently, including multiconfigurational effects in the wave function does not seem to cause a marked change in the optimal geometries.

For a closed-shell singlet state $C_1 \approx 1.0$ and $C_4 = 0.0$ in eq 6. At the other extreme when **B** is predominantly biradical in character $C_1 \approx -C_4$ and the two unpaired electrons, each situated on one anthrone-half, should lead to an observable EPR spectrum. C_1^2 and C_4^2 are a measure of the amount of $|...\ 18b_3\ \overline{18b_3}|$ and $|...\ 18b_2\ \overline{18b_2}|$ configurations, respectively, in the wave function. Thus, when plotted as a function of θ_t, they can be used to assess the extent of the biradical character of **B**. The plot in Figure 4 shows that at $\theta_t = 53°$ and 58.5° (corresponding to the minima of curves b and c in Figure 3) the $X^1\Psi(A)$ wave function is 92.5% and 91.0% $|...\ 18b_3\ 18b_3|$, respectively. Thus one may conclude that **B** is predominantly a closed shell system with no significant biradical character that could lead to an observable EPR spectrum. This occurs because, when θ_t is in the range of 45−60, the HOMO−LUMO gap is sufficiently large that the closed shell ground state is still the best description of the molecule. Consequently, in computing the electron affinities of **B**, a CI open-shell singlet computation is not warranted.

In general, semiquinone radical anions are easily attacked by O_2 to yield the corresponding quinones. Therefore, when performing EPR experiments on semiquinones, care must be used to protect the radicals from O_2 dissolved in the solvent.

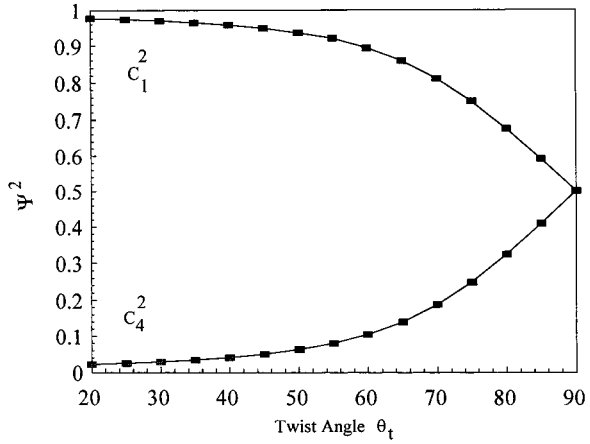

Figure 4. Plot of the C_12 and C_42 terms as a function of the twist angle, θ_t.

However, if the unpaired electron is delocalized over a sufficiently large system, it is conceivable that the semiquinone is stable enough to resist oxidation. This resistance is proportional to the electron affinity (E_a) of the parent neutral quinone. To examine the stability of quinone radical anions as a function of delocalization, the electron affinities of **AQ** and **B** were computed. In addition, to include the effects of the internal reorganizational energies (IRE), the electron affinity was taken as the difference between the optimized heat of formation of the neutral molecule and its anion.

The computed electron affinities for **AQ** and **B** are 1.79 and 3.01 eV. Compared to **AQ**, the delocalization of the unpaired electron over the extra anthrone-half in the $\mathbf{B}^{\bullet-}$ radical increases the E_a of **B** by 1.22 eV. Therefore, the corresponding $\mathbf{B}^{\bullet-}$ might be stable enough to resist oxidation by O_2 in the DMSO solution. The accurate and quantitative estimation of the solvent effects on the E_a of **B** requires the full geometry optimization of the **B** and $\mathbf{B}^{\bullet-}$ surrounded by a large number of DMSO molecules. This is not a trivial task and is beyond our present computational means. However, the actual proof for the stability of $\mathbf{B}^{\bullet-}$, suggested by the E_a computations, must be furnished experimentally.

Figure 5a shows the EPR spectrum of an oxygen-free 1.0 mM solution of the $\mathbf{B}^{\bullet-}$ radical anion after the addition of 1.3 equiv of NaOH in DMSO. Under these conditions, only the $\mathbf{B}^{\bullet-}$ and the $\mathbf{B}^{2-}$ anions are present in solution.[8] This ensures that no exchange broadening mechanism of the type

$$\mathbf{B} + \mathbf{B}^{\bullet-} \rightleftharpoons \mathbf{B}^{\bullet-} + \mathbf{B} \quad (8)$$

or

$$\mathbf{A} + \mathbf{B}^{\bullet-} \rightleftharpoons \mathbf{A}^{\bullet-} + \mathbf{B} \quad (9)$$

exists. The spin exchange broadening due to collisions between the radical anion and the dianion

$$\mathbf{B}^{2-} + \mathbf{B}^{\bullet-} \rightleftharpoons \mathbf{B}^{\bullet-} + \mathbf{B}^{2-} \quad (10)$$

is improbable due to the strong electrostatic repulsion between the two ionic species which have a total of three negative charges.

Under ambient conditions the rate of tumbling of $\mathbf{B}^{\bullet-}$ is very fast compared to the rotational correlation time. Thus the line widths are almost entirely independent of the **g** and hyperfine tensor anisotropies[16] and the spectra appear symmetrical at low and high magnetic fields. Therefore, when simulating a particular spectrum, the peak-to-peak line widths (H_{p-p}) are considered to be constant.

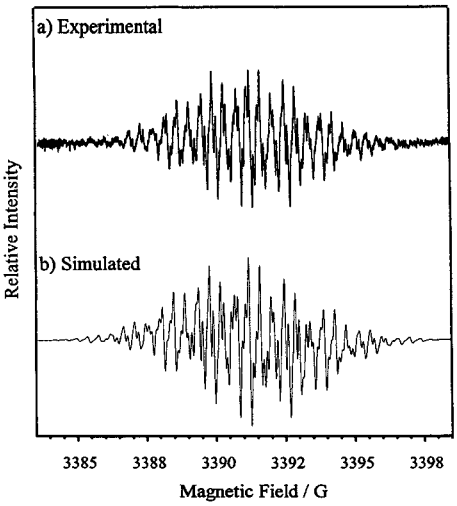

Figure 5. (curve a) Experimental EPR spectrum of the oxygen-free $\mathbf{B}^{\bullet}$ radical anion in basic DMSO: spectrometer frequency = 9.508 Ghz, Microwave power = 210 μW, modulation amplitude = 0.01 G. (curve b) Corresponding simulated spectrum: peak-to-peak line width, H_{p-p} = 0.11 G, average **g** value = 2.0036. The hyperfine coupling constants for the four sets of four equivalent of protons [1,8,1′,8′], [3,6,3′,6′], [2,7,2′,7′] and [4,5,4′,5′] are 1.423, 1.284, 0.405, and 0.385 G respectively.

The simulation of the experimental spectrum is shown in Figure 5b. From this simulation, the total line width in the absence of O_2 $H_{p-p}(0)$ is determined to be 0.11 G. This residual line width broadening is predominantly due to the unpaired electrons of two $\mathbf{B}^{\bullet-}$ radicals exchanging their spin states. Since the exchange is a result of a bimolecular collision, it is concentration dependent. Decreasing the radical concentration would reduce the rate of collisions and give sharper lines. However, due to the large number of hyperfine splittings (625), the lines have low intensities and reducing the concentration would require the use of larger modulation amplitudes. This, in turn, would distort the line shapes and give poor agreement between the experimental and simulated spectra.

Assuming Lorentzian line shapes, an estimate of the second-order rate constant for the radical−radical bimolecular collisions may be obtained from the relation[17]

$$k_2 = \sqrt{3}\gamma_e \Delta H_{p-p}/2[\mathbf{B}^{\bullet-}] \qquad (11)$$

where γ_e is the magnetogyric ratio for the electron. This gives a k_2 value of 1.59×10^9 L mol^{-1} s^{-1}. Since half of the encounters do not lead to an exchange broadening[17], the real k_2 is actually 3.18×10^9 L mol^{-1} s^{-1}. The diffusion-limited k_2 for small radical anions in DMSO is of the order of 5.0×10^9 L mol^{-1} s^{-1}.[18] Thus it is reasonable to conclude that the radical−radical spin exchange is highly probable. It is only hindered by the diffusion of the relatively large $\mathbf{B}^{\bullet-}$ at room temperature and, to a lesser extent, by the interradical anion repulsions.

In the presence of oxygen, the situation is slightly more complicated. Molecular dioxygen has a paramagnetic $^3\Sigma_g^-$ ground state. It has a short-spin lattice relaxation time (T_1) and is considered to be a fast relaxing species. In contrast, the $\mathbf{B}^{\bullet-}$ radical anion has longer relaxation times as evidenced by the narrow line widths and well resolved EPR spectrum in Figure 5a. The Heisenberg spin−spin exchange interaction between fast and slow relaxing species is an effective mechanism for shortening the T_1 of the slow relaxing species.[19] Consequently, the bimolecular collisions between O_2 and $\mathbf{B}^{\bullet-}$ effectively reduce $T_1(\mathbf{B}^{\bullet-})$ and broaden the $\mathbf{B}^{\bullet-}$ EPR line widths. The degree of broadening depends on two factors. The first is the bimolecular collision rate between O_2 and $\mathbf{B}^{\bullet-}$ and the second is the probability P that a Heisenberg spin−spin exchange occurs when a collision takes place.[20]

The frequency of collisions that $\mathbf{B}^{\bullet-}$ is subjected to by O_2 is given by the Smoluchowski equation[20−23]

$$\omega = 4\pi R p[O_2]\{D_S(\mathbf{B}^{\bullet-}) + D_S(O_2)\} \qquad (12)$$

Here R represents the effective interaction distance between $\mathbf{B}^{\bullet-}$ and O_2 while $D_S(\mathbf{B}^{\bullet-})$ and $D_S(O_2)$ are the corresponding local translational diffusion coefficients, when used in this equation.

The peak-to-peak line widths are related to the bimolecular collision rates via the relation[21]

$$\Delta H_{p-p}(O_2) = \frac{2\omega}{\sqrt{3}\gamma_e} = \frac{8\pi R p[O_2]\{D_S(O_2) + D_S(\mathbf{B}^{\bullet-})\}}{\sqrt{3}\gamma_e} \qquad (13)$$

The $D_S(O_2)$ may be obtained from[22]

$$D_S(O_2) = 4.76 \times 10^{-10}(T/\eta) \qquad (14)$$

By using the viscosity η as 0.019 96 P for DMSO[24], $D_S(O_2) = 7.11 \times 10^{-6}$ cm^2 s^{-1} at 25 °C. From the van der Waals volume increments for atoms listed by Edward,[25] the volume of $\mathbf{B}^{\bullet-}$ is estimated to be 461 Å^3, which leads to an effective radius of 4.79 Å. Since the volume of $\mathbf{B}^{\bullet-}$ is larger than that of the DMSO solvent molecules, the Stokes−Einstein equation may be used[25]

$$D = kT/6\pi\eta r \qquad (15)$$

This gives $D_S(\mathbf{B}^{\bullet-}) = 2.28 \times 10^7$ cm^2 s^{-1}. A comparison of these D_S values shows that the value for $\mathbf{B}^{\bullet-}$ is approximately 30 times smaller than that for O_2. Thus $\mathbf{B}^{\bullet-}$ is relatively stationary compared to the rapid motion of O_2 and $D_S(\mathbf{B}^{\bullet-})$ may be neglected in eq 13. In similar cases, such as those of nitroxide spin labels, the D_S values of the slow moving radicals were also neglected.[20−23]

Equation 13 may be rearranged to give

$$Rp = \frac{\sqrt{3}\gamma_e \Delta H_{p-p}(O_2)}{8\pi[O_2]\{D_S(O_2) + D_S(\mathbf{B}^{\bullet-})\}} \qquad (16)$$

The simulated spectrum in Figure 6b was obtained starting from Figure 5b and increasing the H_{p-p} value from 0.11 G in successive increments of 0.01 G. All other parameters were fixed. The best fit was obtained when $H_{p-p}(O_2)$ was 1.30 G. By taking the concentration of a saturated O_2 solution in DMSO to be 2.1 mM,[26] the combined factor Rp is found from eq 16 to be 4.16. It is in very good agreement with the corresponding value of 4.5 for neutral spin labels.[20,23,27] The smaller value is to be expected since in the present case the collisions occur between O_2 and a charged anion. For a neutral spin label, the interaction with the solvent is weak, and collisions between it and O_2 occur frequently. In contrast, a strong solvation sphere of the polar DMSO surrounds the $\mathbf{B}^{\bullet-}$ anion. This impedes the O_2 molecules from closely approaching the $\mathbf{B}^{\bullet-}$ radical where a Heisenberg spin−spin exchange may occur. Thus, although R for $\mathbf{B}^{\bullet-}$ may be 5.0 Å, the protective solvation sphere slightly lowers the effective value of p.

Finally, when the solutions are saturated with dry N_2 and the O_2 is totally expelled, the hyperfine lines regain their sharp line widths with no apparent loss of intensity. This directly proves

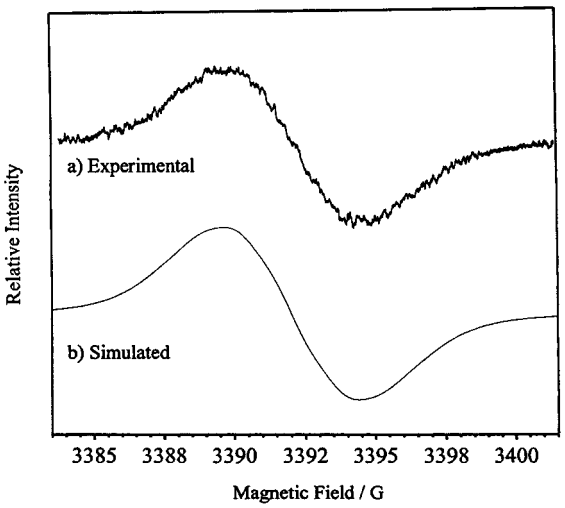

Figure 6. (curve a) Experimental EPR spectrum of the $\mathbf{B}^{\bullet-}$ radical anion in basic DMSO. The sample also contains 2.1 mM of O_2. (curve b) Corresponding simulated spectrum. All experimental settings and simulation parameters, except H_{p-p}, were identical with those of Figure 5. In this case $H_{p-p} = 1.3$ G.

that $\mathbf{B}^{\bullet-}$ does not react chemically with O_2 even when the rate of their encounter in DMSO is quite high.

Summary and Conclusions

The geometry optimization of **A**, $\mathbf{A}^{\bullet-}$, $\mathbf{A}^{2-}$, $\mathbf{A}^{\bullet+}$, $\mathbf{A}^{2+}$, $\mathbf{B}^{\bullet-}$, $\mathbf{B}^{\bullet-}$, $\mathbf{B}^{2-}$, $\mathbf{B}^{\bullet+}$, and $\mathbf{B}^{2+}$ reveals that **A** has the shortest $C_9-C_{9'}$ bond distance and largest $C_9-C_{9'}$ bond order. This is because $\mathbf{A}^{\bullet-}$, $\mathbf{A}^{2-}$, $\mathbf{B}^{\bullet-}$, and $\mathbf{B}^{2-}$ all have occupied HOMOs with antibonding π^* character. Similarly, the $\mathbf{A}^{\bullet+}$, $\mathbf{A}^{2+}$, $\mathbf{B}^{\bullet+}$, and $\mathbf{B}^{2+}$ cations have less than two electrons in their HOMOs which also leads to long bond lengths and small $C_9-C_{9'}$ bond orders.

Keeping both anthrone halves of **B** totally planar during geometry optimization leads to unrealistically high energies at small twist angles. Consequently, its full geometry optimization is required. Figure 3 shows that, at the **B** equilibrium geometry, the singlet state is more stable than the corresponding triplet state. From Figure 4 it is evident that the **B** ground state is predominantly a simple closed-shell singlet with negligible biradical character. Therefore, when computing its equilibrium properties no configuration interaction computations are necessary.

The **B** molecule may be envisaged as two coupled **AQ** molecules that have lost two oxygen atoms. The unpaired electron in the $\mathbf{B}^{\bullet-}$ HOMO is highly delocalized over both anthrone units and causes the radical anion to be very stable. The stability of $\mathbf{B}^{\bullet-}$ is also evident from the computed E_a of **B**. It is 1.22 eV greater than that of **AQ**, which has only one anthrone unit compared to two in **B**.

The relatively high stability of $\mathbf{B}^{\bullet-}$ strongly suggested it might be resistant toward oxidation by O_2 dissolved in solution. This was verified in Figure 6a where an O_2 saturated solution of the radical in DMSO displayed a strong, albeit highly broadened, EPR signal. No evidence for the cleavage of the $C_9-C_{9'}$ bond was observed. Purging this solution with dry N_2 eliminated the O_2 and the normal well resolved EPR signal of $\mathbf{B}^{\bullet-}$ was recovered with no discernible loss in intensity. To the best of our knowledge this is the first semiquinone radical to resist oxidation by O_2.

The line width broadening of $\mathbf{B}^{\bullet-}$ by O_2 was investigated and the effective Rp value between the two species in DMSO at 25 °C was determined to be 4.16. This indicates that the broadening mechanism is slightly less efficient when compared to that of neutral nitroxide spin labels. The lower efficiency is rationalized in terms of a strong solvation sphere surrounding $\mathbf{B}^{\bullet-}$ that decreases the number of successful spin−spin exchange collisions with the O_2 molecules.

From the line width of $\mathbf{B}^{\bullet-}$ in oxygen-free DMSO solutions the rate constant for the spin−spin exchange between two $\mathbf{B}^{\bullet-}$ radicals is found to be 3.19×10^9 L mol^{-1} s^{-1}. This value is close to that expected for a large solvated radical anion diffusing in DMSO solutions at 25 °C.

Acknowledgment. S.M.M. acknowledges the support of the Natural Sciences and Engineering Council of Canada in the form of individual operating and equipment grants. S.M.M. would also like to thank Professor D. H. Evans for useful discussions. We are also grateful to Dr. M. Moller, HyperCube, Inc., for donating the IBM AIX version of the HyperChem software. A.S. and R.S. would like to thank the University of New Brunswick for financial aid in the form of graduate teaching and research assistantships. We are also grateful to Dr. D. G. Sutherland for help with the initial experiments.

References and Notes

(1) Brielbeck, B.; Ruhl J. C.; Evans, D. H. *J. Am. Chem. Soc.* **1993**, *115*, 11898−11903.
(2) Evans, D. H.; O'Connell, K. M. In *Electroanalytical Chemistry. A Series of Advances*; Bard, A. J., Ed.; Marcel Dekker: New York, 1986; Vol. 14, pp 113−207.
(3) Olsen, B. A.; Evans, D. H. *J. Am. Chem. Soc.* **1981**, *103*, 838−843.
(4) Neta, P.; Evans, D. H. *J. Am. Chem. Soc.* **1981**, *103*, 7041−7045.
(5) Brooks, B. R.; Schaefer III, H. F. *J. Am. Chem. Soc.* **1979**, *101*, 307. Nebot, G. I.; Malrieu, J.-P. *J. Am. Chem. Soc.* **1982**, *104*, 3320. Evleth, E. M.; Savin, A. *J. Am. Chem. Soc.* **1981**, *103*, 7414.
(6) Evans, D. H.; Xie, N. *J. Electroanal. Chem.* **1982**, *133*, 367−373.
(7) Evans, D. H.; Xie, N. *J. Am. Chem. Soc.* **1983**, *105*, 315−320.
(8) Mattar, S. M.; Sutherland, D. G. *J. Phys. Chem.* **1991**, *95*, 5129−5133.
(9) Sawyer, D. T.; Roberts, J. L., Jr. *Acc. Chem. Res* **1988**, *21*, 469.
(10) Roberts, J. L., Jr.; Sugimoto, H.; Barrette, W. C.; Sawyer, D. T. *J. Am. Chem. Soc.* **1985**, *107*, 4556.
(11) Sutherland, D. G.; Mattar, S. M. To be published.
(12) HyperChem is a product of Hypercube, Inc., Waterloo, Ontario, Canada. The version used on the IBM RS/6000 work station was kindly donated by Hypercube, Inc.
(13) Stewart, J. P. P. *J. Comput. Chem.* **1989**, *10*, 209. Stewart, J. P. P. *Comput.-Aided Mol. Des.* **1990**, *4*, 1.
(14) Kikuchi, O.; Kawakami, Y. *J. Mol. Struct. (THEOCHEM)*, **1986**, *137*, 365.
(15) Dewar, M. J. S.; Zoebisch, E. G.; Healy, E. F.; Stewart, J. J. P. *J. Am. Chem. Soc.* **1985**, *107*, 3902.
(16) Wilson, R.; Kivelson, D. *J. Chem. Phys.* **1966**, *44*, 154.
(17) Wertz, J. E.; Bolton, J. R. Electron Spin Resonance Elementary Theory and Practical Applications; McGraw-Hill: New York, 1972; pp 198−201.
(18) Gareil, M.; Pinson, J.; Saveant, J. M. *Nouv. J. Chim.* **1981**, 5, 311. Nadjo, L.; Saveant, J. M. *J. Electroanal. Chem.* **1971**, *30*, 41.
(19) Hyde, J. S.; Sarna T. *J. Chem. Phys.* **1978**, *68*, 4439.
(20) Subczynski, W. K.; Hyde, J. S. *Biochim. Biophys. Acta* **1981**, *643*, 283.
(21) Hyde, J. S.; Subczynski, W. K. *J. Magn. Reson.* **1984**, *56*, 125.
(22) Subczynski, W. K.; Hyde, J. S. *Biophys. J.* **1984**, *45*, 743.
(23) Subczynski, W. K.; Hyde, J. S.; Kusumi, A. *Biochemistry* **1991**, *30*, 8578.
(24) Dean, J. A. *Lange's Handbook of Chemistry*, 12th ed.; McGraw-Hill: New York, 1979; p 10−108.
(25) Edward, J. T. *J. Chem. Educ.* **1970**, *47*, 261.
(26) Andrieux, C. P.; Hapiot, P.; Saveant, J. M. *J. Am. Chem. Soc.* **1987**, *109*, 3768.
(27) Windrem, D. A.; Plachy, W. Z. *Biochim. Biophy. Acta* **1980**, *600*, 655.